Energy & Environmental Science

PAPER

View Article Online
View Journal | View Issue

Cite this: *Energy Environ. Sci.*, 2014, **7**, 2329

Operation of lightly doped Si microwires under high-level injection conditions†

Elizabeth A. Santori,[d] Nicholas C. Strandwitz,[d] Ronald L. Grimm,[d] Bruce S. Brunschwig,[a] Harry A. Atwater*[bc] and Nathan S. Lewis*[acd]

The operation of lightly doped Si microwire arrays under high-level injection conditions was investigated by measurement of the current-potential behavior and carrier-collection efficiency of the wires in contact with non-aqueous electrolytes, and through complementary device physics simulations. The current-potential behavior of the lightly doped Si wire array photoelectrodes was dictated by both the radial contact and the carrier-selective back contact. For example, the Si microwire arrays exhibited n-type behavior when grown on a n^+-doped substrate and placed in contact with the 1,1′-dimethylferrocene$^{+/0}$–CH_3OH redox system. The microwire arrays exhibited p-type behavior when grown on a p^+-doped substrate and measured in contact with a redox system with a sufficiently negative Nernstian potential. The wire array photoelectrodes exhibited internal quantum yields of ~0.8, deviating from unity for these radial devices. Device physics simulations of lightly doped n-Si wires in radial contact with the 1,1′-dimethylferrocene$^{+/0}$–CH_3OH redox system showed that the carrier-collection efficiency should be a strong function of the wire diameter and the carrier lifetime within the wire. Small diameter (d < 200 nm) wires exhibited low quantum yields for carrier collection, due to the strong inversion of the wires throughout the wire volume. In contrast, larger diameter wires (d > 400 nm) exhibited higher carrier collection efficiencies that were strongly dependent on the carrier lifetime in the wire, and wires with carrier lifetimes exceeding 5 μs were predicted to have near-unity quantum yields. The simulations and experimental measurements collectively indicated that the Si microwires possessed carrier lifetimes greater than 1 μs, and showed that radial structures with micron dimensions and high material quality can result in excellent device performance with lightly doped, structured semiconductors.

Received 18th January 2014
Accepted 18th March 2014

DOI: 10.1039/c4ee00202d

www.rsc.org/ees

Broader context

Structuring semiconductors on the nano- and microscale is a promising route to enable flexible, lightweight photovoltaics and efficient solar fuels devices. Wire devices with radial junctions should allow for both the efficient absorption of light along the axial dimension of the wire and radial collection of excited photocarriers, therefore enabling the fabrication of efficient devices based on inexpensive materials with low electronic quality. Prior systematic experimental and device physics modeling has largely focused on arrays of doped semiconductors, including Si radial p–n junction devices. The work described herein focuses on the device performance and device physics of lightly doped Si microwires, to allow for new device architectures and increased understanding of devices using other semiconductor materials with less controllable doping.

I. Introduction

Si wire arrays grown by the vapor–liquid–solid (VLS) process have emerged as a promising technology for the fabrication of high efficiency, scalable photovoltaics and artificial photosynthetic devices.[1–6] The photovoltages of Si microwire arrays are not yet comparable, however, to the highest values observed from planar crystalline Si photovoltaics. By analogy to planar Si systems, one approach to improve the photovoltage of the Si microwire arrays would be to operate the system under high-level injection conditions. For lightly doped Si under 1 Sun illumination, the change in the concentration of photogenerated electrons and holes (Δn and Δp, respectively) can

[a]*Beckman Institute, California Institute of Technology, 1200 E. California Blvd., Pasadena, CA 91125, USA. E-mail: nslewis@caltech.edu; Fax: +1 626 395-8867; Tel: +1 626 395-6335*

[b]*Thomas J. Watson Laboratories of Applied Physics, California Institute of Technology, 1200 E. California Blvd, Pasadena, CA, 91125, USA. E-mail: haa@caltech.edu; Fax: +1 626 844-9320; Tel: +1 626-395-2197*

[c]*Member, Kavli Nanoscience Institute, California Institute of Technology, USA*

[d]*Division of Chemistry and Chemical Engineering, California Institute of Technology, 1200 E. California Blvd, Pasadena, CA, 91125, USA*

† Electronic supplementary information (ESI) available: Additional information regarding the VLS growth of Si microwire arrays, photoelectrochemical data correction, photoelectrochemical performance data, and the chemical-mechanical polishing of Si microwire arrays. See DOI: 10.1039/c4ee00202d

greatly exceed the equilibrium carrier concentrations in the dark (n_0 and p_0, respectively). For such samples operated under high-level injection conditions, the Shockley–Read–Hall recombination rate is inversely proportional to the sum of both the carrier lifetimes. The high-level lifetime is therefore longer than the lifetime under low-level injection conditions for a doped semiconductor, whose carrier lifetime is essentially equal to the minority-carrier lifetime.[7,8]

Planar devices operating under high-level injection conditions, such as Si point-contact solar cells, have achieved the highest efficiencies for a single-junction Si photovoltaic cell, with cell efficiencies >27% under concentrated solar illumination.[9–11] These devices utilize lightly doped, float-zone Si, and are fabricated with small interdigitated n^+ and p^+ back point-contacts, to facilitate the selective collection of electrons and holes, respectively. Such devices do not have significant electric fields in the bulk of the semiconductor, and the photogenerated carriers are therefore driven by diffusion, not drift, within the bulk of the material. Accordingly, the Si must possess an extremely long (>1 ms) charge-carrier lifetime, and high-quality surface passivation on both the front and back of the cell is necessary to minimize recombination losses at the surfaces of the device. The n^+ and p^+ point contacts generate strong electric fields at the contacts, and thus facilitate the collection of photogenerated carriers, in addition to creating low saturation currents in the device. This highly optimized structure also benefits from having a highly reflective back surface, an anti-reflection coating on the front surface, and no shadowing due to the lack of a top contact.

In this work, we describe the operation of Si microwire arrays under high-level injection conditions. Non-aqueous redox couples with varying electrochemical potentials, including the 1,1′-dimethylferrocene $(Me_2Fc)^{+/0}$–CH_3OH and cobaltocene $(CoCp_2)^{+/0}$–CH_3CN redox systems, have been used to systematically probe the current density *vs.* potential, *J–E*, behavior of the wire arrays and to compare their behavior with the *J–E* properties of point-contact planar Si systems operated under nominally the same conditions.[12,13] The $Me_2Fc^{+/0}$–CH_3OH and $CoCp_2^{+/0}$–CH_3CN systems have both been shown to generate an inversion layer in contact with Si, resulting in semiconductor/liquid interfaces that have a high selectivity for holes and electrons, respectively, as well as low effective surface recombination velocities, *S*.[14]

The lightly doped Si microwires are expected to be depleted in contact with the chosen redox couples, given the acceptor concentrations $N_A \sim 1 \times 10^{13}$–$1 \times 10^{14}$ cm^{-3} and diameters $d \sim$ 2.5–3.0 μm of the microwires. Previous device physics simulations of doped Si microwires predicted that depleted wires (*i.e.* wires with small internal electric fields, for which a fully developed space-charge length would exceed the radius of the wire) should have extremely low carrier-collection efficiencies, due to the absence of a significant electric field within the wire and the lack of majority carriers to facilitate axial carrier transport.[15–17] These simulations exclusively examined the performance of doped wires with radii on the order of the depletion width of the wire, *i.e.* $r \sim 100$ nm for $N_A = 1 \times 10^{18}$ cm^{-3}. For Si microwires in contact with $Me_2Fc^{+/0}$–CH_3OH, the near-surface region of the wire is expected to be strongly inverted, as demonstrated previously for planar n-Si/$Me_2Fc^{+/0}$–CH_3OH junctions.[14,18,19] Although the lightly doped Si microwires should be depleted, their radii are potentially large enough such that the wires could still possess an electric field due to the large concentration of holes at the surface relative to the wire core, thereby allowing for selective carrier collection. Thus, further quantitative modeling of lightly doped, structured materials is required to fully understand the device properties of these systems.

A focus of the work described herein was to experimentally measure the external and internal quantum yields of such Si microwires using non-aqueous photoelectrochemical redox systems. Previous measurements of undoped Si microwire array photoanodes in contact with $Me_2Fc^{+/0}$–CH_3OH have shown non-unity carrier collection efficiencies.[20] Some possible explanations for this effect include the presence of Cu silicide located at the tops of the wires, as well as an inherently poor carrier collection in lightly doped Si wires. To distinguish between these possibilities, the Cu silicide located at the tops of the wires was removed through chemical-mechanical polishing of the wire arrays, and the internal quantum yield, Γ_{int}, of the wire array photoelectrodes was subsequently measured.

In addition, device physics models were developed for the operation of lightly doped Si wires with a selective n^+ back contact, in radial contact with the $Me_2Fc^{+/0}$–CH_3OH electrolyte. The internal quantum yield of a single wire has been simulated as a function of: the distance, d_T, between the location of carrier excitation and the top of the wire; the lifetime and carrier concentration in the wire; and the wire diameter, *d*. This type of 'scanning' simulation was preferred to a measurement of the full spectral response or the *J–E* characteristics of a single wire, because the actual excitation profile is not well known either for wires with diameters on the microscale or for arrays of wires. The absorption profile differs significantly from that of planar Si, and should also vary considerably for wires with radial dimensions ranging from nanometers to microns.[21] Hence, a scanning illumination measurement effectively removes the unknown variable of the excitation profile within the wire, and allows measurement of the efficiency of carrier-collection at each point along the axial direction of a single Si wire.

II. Experimental section

A. Reagents

Methanol (BakerDRY, Mallinckrodt Baker) and lithium perchlorate (battery grade, Sigma-Aldrich) were used as received. 1-1′-dimethylferrocene (Me_2Fc, 95%, Sigma-Aldrich) was purified by sublimation at room temperature, and dimethylferrocenium tetrafluoroborate (Me_2FcBF_4) was synthesized as described previously.[22] Acetonitrile (99.8% anhydrous, Sigma-Aldrich) was purified first by sparging with N_2(g) for 15 min, and then passing the solvent, under pressure from N_2(g), through a column of activated A2 alumina (Zapp's). Bis(cyclopentadienyl)cobalt(II) ($CoCp_2$, 98%, Strem) was purified by vacuum sublimation at 65 °C. Cobaltocenium hexafluorophosphate (Cp_2CoPF_6, 98%, Sigma-Aldrich) was

recrystallized from an ethanol/acetonitrile mixture (ACS grade, EMD) and dried under vacuum. VLS-catalyzed Si microwire arrays were grown on both n^+- and p^+-doped (111)-oriented Si substrates, using degenerately doped n^+-Si substrates with a resistivity $\rho \sim 0.001$–0.004 Ω cm and 450 nm of thermal oxide (University Wafer), or p^+-Si substrates with $\rho \sim 0.001$–0.005 Ω cm and 500 nm of thermal oxide (International Wafer Service).

B. VLS-catalyzed microwire growth

Arrays of square-packed Si microwires were grown on oxide-coated, lithographically patterned, planar n^+- and p^+-Si(111) substrates using the vapor–liquid–solid (VLS) growth method with a Cu catalyst (99.9999%, ESPI) and without dopants (see ESI†).[20] For photoelectrochemical measurements under 1 Sun of light intensity, the resulting undoped wires grown on an n^+-Si substrate (n^+/i-Si microwires) were 2.7–2.9 μm in diameter and 67–80 μm in height (Fig. 1). The p^+/i-Si microwires were 1.65–1.75 μm in diameter and 90–97 μm in height. The n^+/i-Si wires that were measured for their spectral response and optical properties were 2.1–2.3 μm in diameter and 65–75 μm in height. After wire growth, the Cu VLS catalyst was removed by a 5 s buffered HF(aq) (BHF, Transene Inc.) etch, followed immediately by an etch in 6 : 1 : 1 (by volume) of H_2O : HCl : H_2O_2 at 70 °C (RCA 2) for 15 min. This BHF/RCA2 procedure was then repeated to ensure that all of the metal catalyst had been removed.

Four-point resistance measurements on single wires were performed as described previously, for wires grown on both n^+- and p^+-Si substrates.[20,23] The undoped Si microwires had a resistivity of 800 ± 500 Ω cm as grown on n^+ substrates and a resistivity of 200 ± 100 Ω cm as grown on p^+ substrates. For wires grown on either n^+ and p^+-Si substrates, gate-dependent conductance measurements indicated that the microwires were slightly p-type, and showed an increase in conductivity with a negative applied gate-bias. The as-grown microwires thus possessed low electronically active acceptor concentrations, N_A, of $\sim 1 \times 10^{13}$–1×10^{14} cm^{-3}.

C. Electrode fabrication

To fabricate multiple electrodes for photoelectrochemical measurements, arrays of Si microwires were cleaved into ~4 × 4 mm samples. A SiC scribe was used to scratch Ga : In eutectic into the backs of the samples, thereby producing an ohmic contact to the Si substrate. Ag print (GC Electronics) was then used to affix the samples to a coiled wire that had been passed through a glass tube, with the resulting electrode positioned in a face-down configuration. A low-creep epoxy (Loctite 9460 F) was used to define the active area of the electrode, and a higher stability epoxy (Hysol 1C) was used to encapsulate the back contact and wire coil. The electrodes were placed for 4 h in an oven heated to 70 °C, to further cure the epoxy, thereby obtaining enhanced chemical stability in both the CH_3OH and CH_3CN solutions. The electrode areas were ~0.03 cm^2, as measured using a high-resolution scanner and analyzed by Adobe Photoshop software.

D. Photoelectrochemical Measurements

All non-aqueous photoelectrochemical *J–E* measurements were performed with bottom illumination in air-tight, flat-bottomed glass cells. The $Me_2Fc^{+/0}$–CH_3OH electrolyte solution consisted of 200 mM of Me_2Fc, 0.4 mM of Me_2FcBF_4, and 1.0 M $LiClO_4$ in 30 mL of methanol. The cell was assembled and sealed under an inert atmosphere (<10 ppm O_2), and subsequently was placed under positive Ar(g) pressure on a gas manifold. A high surface-area Pt mesh was used as the counter electrode, and the reference electrode was a Pt wire in a Luggin capillary that had been filled with the same solution as that in the main cell compartment. The difference between the Nernstian potential of the solution and the potential of the reference electrode was recorded using a 4-digit voltmeter (Keithley), with the value differing from the reference electrode potential by <10 mV. *J–E* measurements were obtained at a scan rate of 5 mV s^{-1}.

The $CoCp_2^{+/0}$–CH_3CN electrolyte solution consisted of 50 mM of $CoCp_2PF_6$, 5.0 mM of $CoCp_2$, and 1.0 M $LiClO_4$ in 20 mL of acetonitrile. The cell was assembled and used under an inert, dry atmosphere (<0.50 ppm O_2; 0.5 ppm H_2O). A high surface-area Pt mesh was used as the counter electrode, and the reference electrode was a Pt wire that was placed in the solution in close proximity to the working electrode. A Luggin capillary was not used as a reference electrode in this cell, due to the instability and relatively low concentrations of $CoCp_2$ in the electrolyte. *J–E* measurements were obtained at a scan rate of

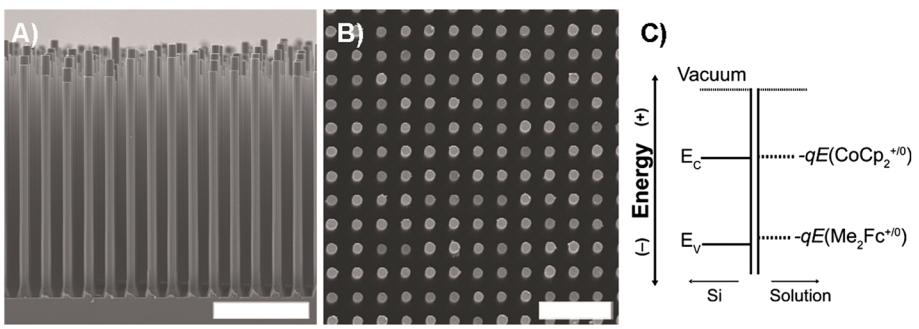

Fig. 1 (A) Side view scanning electron microscopy image of a cleaved array of square-packed Si microwires. Scale bar = 30 μm. (B) Top view of the same Si microwire array. Scale bar = 20 μm. (C) Energy *versus* position diagram for Si and two liquid electrolytes, $Me_2Fc^{+/0}$–CH_3OH and $CoCp_2^{+/0}$–CH_3CN, before contact.

30 mV s^{-1}, to limit the solution optical absorption produced by the generation of $CoCp_2$ at the working electrode.

A 300 W ELH-type tungsten-halogen bulb with a dichroic rear reflector and diffuser was used as the illumination source for electrochemical measurements under simulated 1 Sun illumination in contact with $Me_2Fc^{+/0}$–CH_3OH or $CoCp_2^{+/0}$–CH_3CN. The incident light intensity was calibrated using a Si photodiode that was placed in the solution at the position of the working electrode. The light intensity was adjusted until the short-circuit photocurrent of the Si diode was the same as the short-circuit photocurrent produced on the photodiode by 100 mW cm^{-2} of AM 1.5G illumination. The Si electrodes were etched for 5 s in 5% HF(aq), rinsed with >18 MΩ cm resistivity H_2O, and dried thoroughly under a stream of N_2(g) prior to photoelectrochemical measurements. The electrochemical cell solutions were vigorously stirred during the *J–E* measurements. Data were collected and averaged for seven wire array samples each, for wire array photoelectrodes tested in $Me_2Fc^{+/0}$ and $CoCp_2^{+/0}$ electrochemical cells.

To reduce the concentration overpotential losses within the $Me_2Fc^{+/0}$–CH_3OH cell and to demonstrate the validity of the corrections for these losses, *J–E* measurements were also performed for electrolytes that had 40 mM Me_2FcBF_4 added to the cell (see ESI† for calculations). The cells were illuminated using a 1 W 808 nm diode laser (Thorlabs), and *J–E* data were collected by matching the short-circuit photocurrent density, J_{sc}, to the value of J_{sc} that was obtained under 1 Sun ELH-type W-halogen illumination for each electrode. This process required ~55 mW cm^{-2} of 808 nm illumination, as measured by a calibrated Si photodiode (FDS-100, Thorlabs) placed in the electrochemical cell at the position of the working electrode.

To determine the diode quality factor of the Si microwire photoelectrodes in contact with $Me_2Fc^{+/0}$–CH_3OH, the *J–E* behavior was measured at a series of light intensities under 808 nm illumination. At each light intensity, the open-circuit photovoltage, V_{oc}, was initially measured using a Keithley 4-digit voltmeter, and the J_{sc} was measured from the *J–E* behavior of the electrode. The V_{oc} is expected to the have the general form:

$$V_{oc} = \frac{nkT}{q}\ln\left(\frac{J_{ph}}{J_0}\right) \quad (1)$$

where n is the diode quality factor, k is Boltzmann's constant, T is the absolute temperature, q is the unsigned charge on an electron, J_{ph} is the photocurrent density, and J_0 is the dark saturation current density.[24] Therefore, a plot of V_{oc} *versus* $\ln(J_{ph})$ should be linear with a slope of nkT/q, allowing for the determination of the value of n. To calculate the diode quality factor, the behavior of the n^+/i-Si microwire array photoelectrodes was measured under 808 nm illumination ranging in light intensity from ~13 mW cm^{-2} to 165 mW cm^{-2}, corresponding to ~0.24–3.0 Suns of illumination.

E. Angle-resolved spectral response and optical measurements

Angle-resolved spectral response and optical measurements of Si microwire arrays were obtained as described previously, using a chopped (f = 30 Hz) Fianium supercontinuum laser coupled to a monochromator, in conjunction with two rotational stages that permitted rotation of the sample around both the θ_x and θ_y axes.[20,25] The angle-resolved spectral response measurements were obtained using side-facing electrodes of high-fidelity Si microwire arrays, with overall electrode dimensions of ~7 mm × 7 mm. The electrodes were fabricated so that the Si microwire arrays would ultimately be eucentric with respect to the rotational axes, θ_y and θ_x. The $Me_2Fc^{+/0}$–CH_3OH electrochemical cell contained a solution of 10 mM of Me_2Fc, 0.4 mM of Me_2FcBF_4, and 1.0 M $LiClO_4$ in 25 mL of methanol, and was maintained under a positive pressure of Ar(g) during the experiments. The photoelectrode was aligned in the cell by utilizing the reflected optical diffraction pattern, and normal incidence ($\theta_{x,y}$ = 0°) was determined by minimizing the photocurrent of each electrode. A calibrated Si photodiode (FDS-100, Thorlabs) that was positioned inside the cell was used to calculate the external quantum yield, Γ_{ext}, of the Si microwire array photoelectrodes.

An integrating sphere was used to perform optical transmission and reflection measurements as a function of the wavelength (λ) and incident angle of illumination on peeled-off films of Si microwires embedded in polydimethylsiloxane (PDMS; Sylgard 184, Dow Corning).[25] Optical measurements were made on peeled arrays formed using pieces of the Si microwire array that were adjacent to the pieces used for measurement of the spectral response. Because the heights of the wires can vary considerably across one growth chip, care was taken to measure wires with the same heights for the optical and photoelectrochemical measurements, by using adjacent portions of the same array, with the samples located at equal distances from the growth front on the chip. The optical diffraction patterns of the arrays were used to orient the films relative to the rotational axes (θ_x, θ_y). The maximization of transmission in the films was taken to indicate normal incidence to the wire array.

To determine the effect of the Cu silicide region on the carrier-collection efficiency of undoped Si microwires, the Cu-rich region, located at the tops of the wires, was selectively removed by chemical-mechanical polishing. Arrays of n^+/i-Si microwires were fully embedded with mounting wax and subsequently polished by hand using powder Al_2O_3 and silica suspensions (see ESI†). Half of each array was reserved as a control, to provide a direct comparison for spectral response and optical measurements, respectively, between the same wires in the measurements of polished and unpolished electrodes and films.

F. Device physics simulations

Device physics simulations were performed using Sentaurus Device software (Synopsis Inc.). Wires were defined in two dimensions (2D) using cylindrical coordinates. The contacts for the wire included the high barrier-height contact, which was applied radially to the wire, and an n^+-doped back-surface field that acted as an electron-selective contact. The wires were n-type, with dopant densities N_D varying from $N_D = 1 \times 10^{11}$ to $N_D = 3 \times 10^{19}$ cm^{-3}. The radial liquid contact was simulated

using a Schottky-type contact that formed a high barrier-height (*i.e.*, a Fermi level of $\mathbf{E}(A/A^-) = 5.15$ eV and an electron affinity of Si $\mathbf{E}_{A\ Si} = 4.05$ eV) with n-Si, with Si dopant densities as indicated in the text. The surface recombination velocity for electrons and holes was set to 100 cm s^{-1} at the radial contact, to approximate a semiconductor/liquid contact using outer-sphere redox couples.[16] The distance $d_T = 0$ μm was defined to be the top of the wire (far from the n^+ back-surface field), and the wire was 70 μm in length. The n^+ back-surface field was defined from $d_T = 69.5$–70 μm, and consisted of an n^+ layer with a donor concentration $N_D = 1 \times 10^{18}$ cm^{-3}. Electron and hole surface recombination velocities at the back contact were set to 1×10^7 cm s^{-1}. The dopant density was uniform throughout the wire, except at the base of the wire where the back-surface field was present. Scanning photocurrent simulations were conducted by scanning a simulated light beam ($\lambda = 250$ nm) axially along a wire from $d_T = 0$–70 μm. The spot size was 100 nm and the photon flux was very low, having a value of 6.245×10^{15} photons cm^{-2} s^{-1}. Because of the high barrier height and the high concentration of holes, this photon flux did not perturb the hole concentration from the equilibrium value for undoped wires. The quantum yield for carrier collection at zero applied voltage was determined by integrating the total number of excitations per unit time in the wire and dividing that quantity into the number of electrons collected per unit time derived from the current at the contacts. The simulation grid was set to a minimum mesh size of 100 nm. The refined mesh was narrowed linearly to 1 nm near the contacts as well as at the interface between the wire bulk and the n^+-doped back surface field. The carrier mobilities were taken to have bulk values (1470 cm^2 V^{-1} s^{-1} and 470.5 cm^2 V^{-1} s^{-1} for electrons and holes, respectively) that decreased with increasing dopant densities according to empirically developed and well-established relationships for Si.[26] Measurements of the Hall mobility in single crystalline Si have shown no substantial change after Cu incorporation.[27] The concentration of electronically active interstitial Cu should be approximately 1×10^{13}–1×10^{15} cm^{-3} after the growth period[27,28] and thus the present ionized impurities should not have a substantial effect on the carrier mobility. A Shockley–Read–Hall lifetime was set for each simulation ($\tau_n = \tau_p$), and the value was adjusted based on the empirical relationship with the dopant density given in eqn (2):

$$\tau_{SRH} = \frac{\tau_n}{\left(1 + \frac{N}{N_{ref}}\right)} \quad (2)$$

where N is the dopant density, $N_{ref} = 1 \times 10^{16}$ cm^{-3}, τ_n is the initial value set for the carrier lifetime, and τ_{SRH} is the final value used in the computation of the recombination rates.

III. Results

A. Photoelectrochemical behavior of lightly doped Si microwire arrays in contact with $Me_2Fc^{+/0}$–CH_3OH and $CoCp_2^{+/0}$–CH_3CN electrolytes

Fig. 2 shows the *J*–*E* behavior of the n^+/i-Si and p^+/i-Si microwire array photoelectrodes in contact with $Me_2Fc^{+/0}$–CH_3OH under

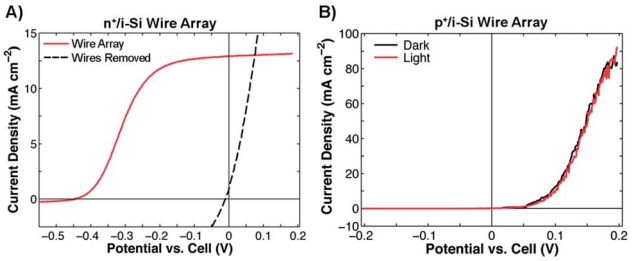

Fig. 2 Uncorrected *J*–*E* behavior of (A) n^+/i-Si and (B) p^+/i-Si microwire arrays in contact with $Me_2Fc^{+/0}$–CH_3OH under 100 mW cm^{-2} of ELH-type W halogen illumination, and in the dark.

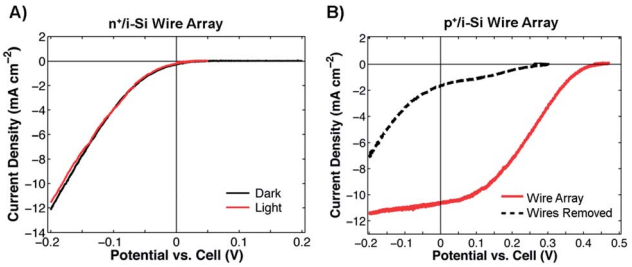

Fig. 3 Uncorrected *J*–*E* behavior of (A) n^+/i-Si and (B) p^+/i-Si microwire arrays in contact with $CoCp_2^{+/0}$–CH_3CN under 100 mW cm^{-2} of ELH-type W halogen illumination, and in the dark.

1 Sun of simulated solar illumination. The n^+/i-Si microwire electrodes exhibited $V_{oc} = 445 \pm 13$ mV, $J_{sc} = 12.8 \pm 2.1$ mA cm^{-2}, fill factors ff of 0.41 ± 0.03, and photoelectrode energy-conversion efficiencies η of $2.3 \pm 0.3\%$. In contrast, the p^+/i-Si microwire array photoelectrodes showed no photoresponse in contact with this electrolyte. For all electrodes, the degenerately doped growth substrates did not significantly contribute to the measured photoresponse of the wire arrays, as indicated by measurement of the photoresponse of the electrodes with the wires removed from the substrate through use of non-abrasive mechanical force (see Table S1 in ESI† for all figures of merit).

Fig. 3 shows the photoresponse of the same n^+/i-Si and p^+/i-Si microwire array electrodes measured in contact with the $CoCp_2^{+/0}$–CH_3CN electrolyte. The p^+/i-Si electrodes behaved as photocathodes in contact with the $CoCp_2^{+/0}$ redox couple, exhibiting $V_{oc} = 421 \pm 14$ mV, $J_{sc} = 10.9 \pm 0.3$ mA cm^{-2}, ff = 0.32 ± 0.02, and $\eta = 1.5 \pm 0.1\%$. Consistent with measurements of p^+/i-Si arrays in contact with $Me_2Fc^{+/0}$–CH_3OH, the n^+/i-Si arrays showed no photoresponse in contact with $CoCp_2^{+/0}$–CH_3CN.

To reduce parasitic losses from concentration overpotential effects within the cell, the *J*–*E* response of the n^+/i-Si microwire electrodes was also measured in contact with $Me_2Fc^{+/0}$–CH_3OH in the presence of a higher concentration of the oxidized form of the redox couple, Me_2Fc^+. Under these conditions, the n^+/i-Si microwire photoelectrodes exhibited fill factors of $ff_{808\ nm} = 0.58 \pm 0.02$ and an efficiency $\eta_{808\ nm} = 5.9 \pm 1.0\%$ under 55 mW cm^{-2} of 808 nm illumination, along with diode quality factors of $n = 1.90 \pm 0.07$ (Fig. 4). After correcting the *J*–*E* data for losses due to concentration overpotential and uncompensated cell

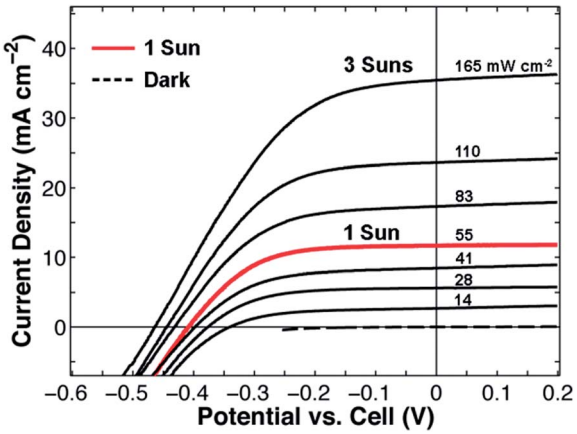

Fig. 4 Uncorrected J–E data as a function of illumination intensity (labeled in units of mW cm^{-2}) at 808 nm for a representative n$^+$/i-Si microwire array photoelectrode in contact with 200 mM Me_2Fc/40 mM Me_2FcBF_4 in CH_3OH.

resistances, which contribute to the low fill factors of the measured wire arrays, the corrected fill factor and photoelectrode efficiency values for electrodes measured under 1 Sun of simulated solar illumination were $ff_{corr} = 0.62 \pm 0.04$ and $\eta_{corr} = 3.5 \pm 0.6\%$, respectively (Fig. S1†).

To investigate the carrier-collection efficiency of the lightly doped Si microwire arrays, measurements of the external and internal quantum yields were performed on n$^+$/i-Si photoelectrodes in contact with $Me_2Fc^{+/0}$–CH_3OH. Given the anisotropy of light absorption within an array with respect to the angle of incident illumination, the spectral response and optical measurements were performed at normal incidence.[25] The maximum external quantum yield of the n$^+$/i-Si photoelectrodes was $\Gamma_{ext} \sim 0.23$ under visible illumination. Measurements of the external quantum yield with respect to wavelength displayed oscillations, which have been previously attributed to whispering-gallery modes within the cylindrical Si microwires.[20] The maximum internal quantum yield was $\Gamma_{int} \sim 0.79$ (Fig. 5), in good agreement with previous measurements on undoped Si microwire array photoanodes.[20] Both Γ_{ext} and Γ_{int} showed no change between as-grown wires that contained the Cu silicide region near the top of the wires, and polished wires for which the silicide had been removed. Thus, for the undoped Si microwire arrays, the presence of the interfacial region at the tops of the wires had no measurable effect on the carrier-collection efficiency within the wires.

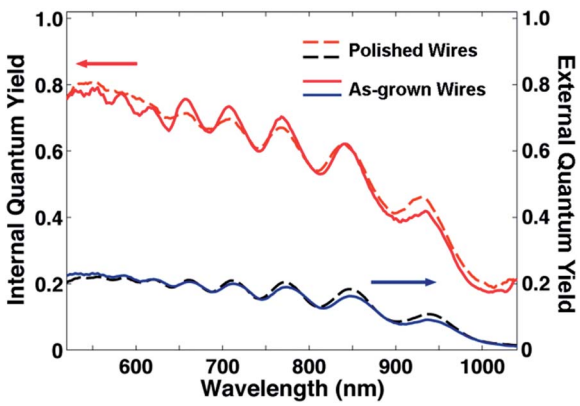

Fig. 5 External quantum yield and internal quantum yields of as-grown and polished n$^+$/i-Si microwire array photoelectrodes, measured in contact with $Me_2Fc^{+/0}$–CH_3OH.

B. Device physics model of the photoelectrochemical behavior of n$^+$i-Si microwires in contact with $Me_2Fc^{+/0}$–CH_3OH

The carrier concentration within a single n$^+$/i-Si microwire while in contact with $Me_2Fc^{+/0}$–CH_3OH in the dark at zero applied bias was simulated using Sentaurus Device. For either $d = 0.10$ μm or $d = 2.4$ μm, the lightly doped n-Si wires with $N_D = 1 \times 10^{13}$ cm^{-3} had high concentrations of holes throughout the volume of the wires (Fig. 6). The smaller diameter $d = 0.10$ μm wire was simulated to be strongly inverted, with a background concentration of holes exceeding 1×10^{16} cm^{-3} within the core and approaching 5×10^{18} cm^{-3} at the surface of the wire. The larger diameter $d = 2.4$ μm wire was simulated to be more weakly inverted, but still possessed hole carrier concentrations in the wire core that exceeded the background concentration of carriers in the wire when not in contact with Me_2Fc–CH_3OH. Within the simulations, the radial contact determined the equilibrium concentration of carriers; thus, the results were also directly applicable to the experimental system, in which the wires are slightly p-type, with either n$^+$ or p$^+$ contacts.

The carrier-collection efficiency within a single wire was simulated for a wire with $d = 2.4$ μm, with the doping density varying from $N_D = 1 \times 10^{11}$ to $N_D = 3 \times 10^{19}$ cm^{-3} (Fig. 7). The Shockley–Read–Hall lifetime was fixed at a value of $\tau_{SRH} = 1$ μs, which corresponds to an effective diffusion length, L_{eff}, for electrons of ~60 μm, assuming an electron mobility of $\mu_e \sim 1400$ cm^2 V^{-1} s^{-1}. This lifetime was a realistic value for a first simulation, given that L_{eff} values ranging from 10 μm to >30 μm have been measured for single-wire Si p–n junctions under low-level injection conditions.[3] The use of this particular lifetime also assured that, for the fixed d employed, radial collection would be unity for moderately doped wires, in agreement with previous work on the behavior of radial p–n junctions.[29] However, for wires with $N_D < 1 \times 10^{15}$ cm^{-3}, the simulated carrier-collection efficiency deviated from unity, particularly for

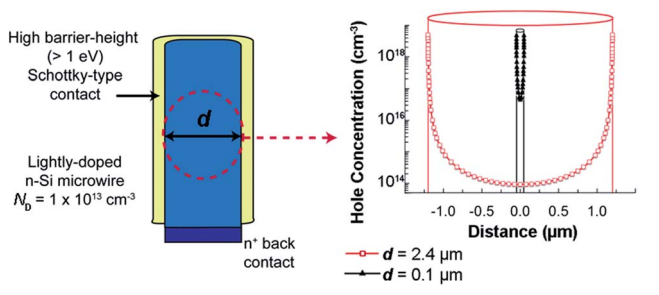

Fig. 6 Concentration of holes within a single undoped Si wire in contact with $Me_2Fc^{+/0}$–CH_3OH in the dark, as a function of the distance radially within the wire, for two different wire diameters, $d =$ 0.10 μm and $d = 2.4$ μm.

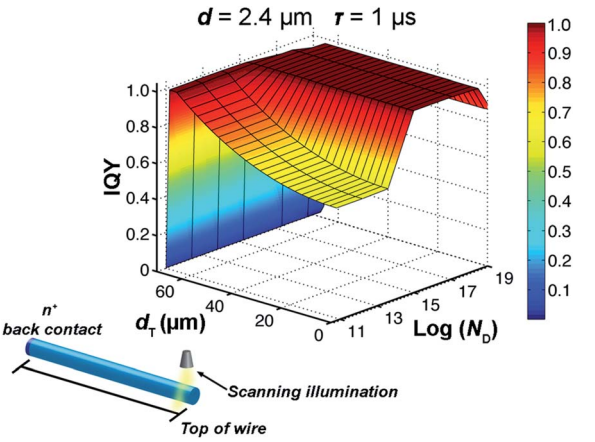

Fig. 7 Variation of the carrier-collection efficiency along the axial direction of a single Si microwire with a dopant density N_D, with a diameter $d = 2.4$ μm and a charge-carrier lifetime of 1 μs. Included is a schematic of the scanning internal quantum yield simulation for a single Si wire, with the internal quantum yield simulated as a function of the distance of the excitation from the top of the wire.

carriers generated at the top of the wire. This result can be understood in view of the carrier concentration within the wire; under the simulation conditions, the n-type wires were fully inverted, with a background concentration of holes greater than the background concentration of electrons, resulting in an increase in the recombination rate for electrons within the wire. The photogenerated electrons must be transported down the length of the wire to be collected at the back contact, but will have a high probability of recombining with the large concentration of holes throughout the wire. Thus, under these simulation conditions, the performance of this device architecture was limited by electron transport down the length of the wire. Wires with $N_D \sim 1 \times 10^{15}$–$1 \times 10^{18}$ cm^{-3} were simulated to exhibit $\Gamma_{int} = 1$, in agreement with previous simulations for wires with radii $R < L_{eff}$. For wires with N_D exceeding $\sim 5 \times 10^{18}$ cm^{-3}, other recombination mechanisms, such as Auger recombination, began to dominate the carrier dynamics, decreasing the overall lifetime and ultimately limiting the radial collection of carriers.

The carrier-collection efficiency within a single, lightly doped wire was also simulated as a function of the radius of the wire and the Shockley–Read–Hall lifetime of the Si (Fig. 8). Variation of either parameter had a significant effect on the internal quantum yield. For wires with $d < 200$ nm, the carrier-collection efficiency decreased precipitously relative to wires that had larger diameters. This result is consistent with the expected complete depletion of electrons within the wire at these diameters, and with the presence of a hole-rich inversion layer in the near-surface region that extended ~100 nm in depth into the wires. At such small radii, the wires are strongly inverted throughout the radial dimension, resulting in high recombination rates for electrons traversing the length of the wire.

The internal quantum yield also exhibited a significant dependence on the carrier lifetime within the range of 1–10 μs, with Γ_{int} approaching values >0.9 in wires with $\tau_{SRH} = 10$ μs.

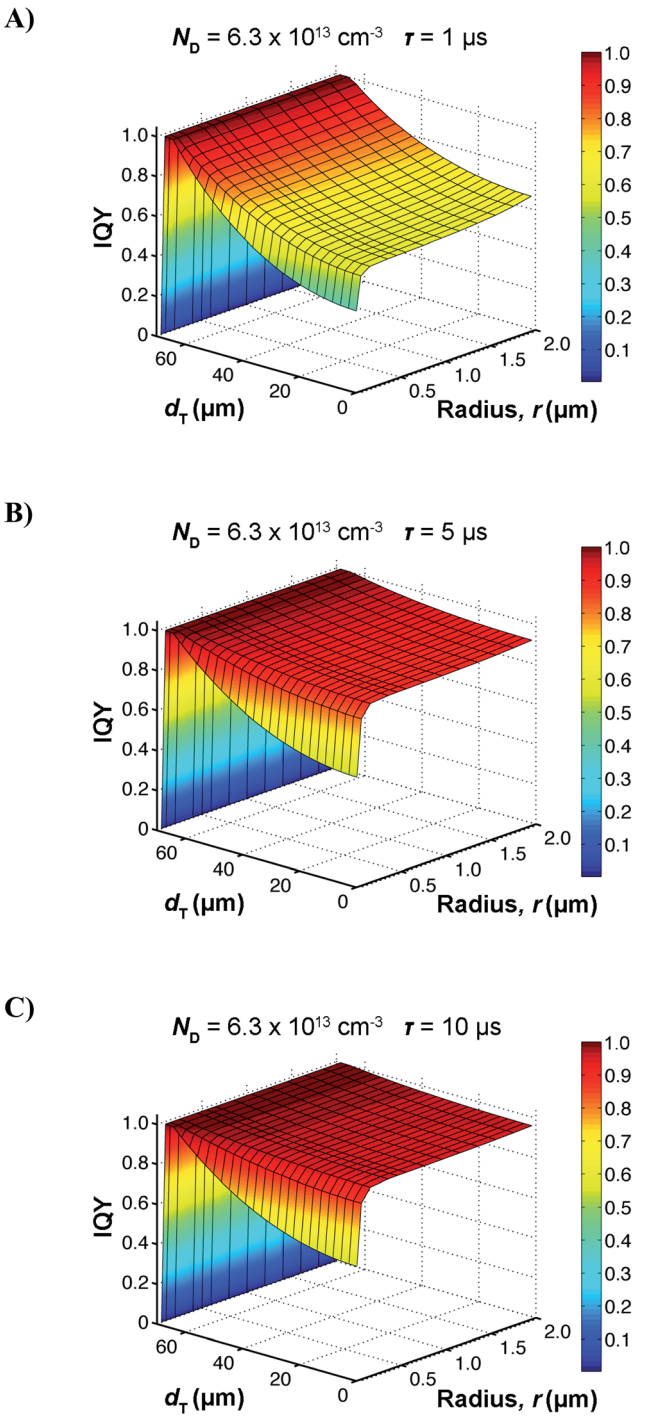

Fig. 8 Variation of the carrier-collection efficiency along the axial direction of a single wire with respect to the radius of the wire, for a dopant density $N_D = 6.3 \times 10^{13}$ cm^{-3} and charge-carrier lifetimes of (A) 1 μs, (B) 5 μs, and (C) 10 μs.

Assuming an electron mobility of $\mu_e \sim 1400$ cm^2 V^{-1} s^{-1}, this range of lifetimes corresponds to $L_{eff} = 60$–190 μm. Thus, to collect the majority of carriers in a 70 μm long wire, the effective diffusion length must be significantly greater than the length of the wire. Even though the device was structured to facilitate the radial collection of carriers, the axial transport of electrons

ultimately limits the carrier-collection within the device, necessitating the use of a material with a large diameter as well as a long carrier diffusion length.

IV. Discussion

A. Current-potential behavior of Si microwire arrays under high-level injection

Although the lightly doped Si microwires investigated herein were expected to be depleted, the n^+/i-Si wire arrays in contact with $Me_2Fc^{+/0}$–CH_3OH yielded efficiencies and fill factors that were very similar to those observed for optimally doped p-Si wire array photocathodes in contact with $MV^{2+/+}$(aq).[30,31] The demonstrated photovoltages of the n^+/i-Si wire arrays exceeded the bulk recombination/diffusion-limited V_{oc} under low-level injection conditions of V_{oc} = 392 mV, calculated from eqn (3):[32,33]

$$V_{oc} = \frac{kT}{q}\ln\left(\frac{J_{ph}\,L_n N_A}{qD_n n_i^2}\right) \quad (3)$$

where k is Boltzmann's constant, T is the absolute temperature (298 K), q is the unsigned elementary charge, J_{ph} is the light-limited photocurrent density (12.8 mA cm^{-2}), D_n is the diffusion coefficient of minority carriers (36 cm^2 s^{-1}), L_n is the minority-carrier diffusion length ($L_n = 13.4$ μm, where $L_n = \sqrt{D_n \tau_n}$ and τ_n = 5 μs), N_A is the dopant density (3×10^{13} cm^{-3}), and n_i is the intrinsic carrier concentration (1.45×10^{10} cm^{-3}) of the semiconductor. A V_{oc} exceeding the 392 mV value can only be achieved if the injected majority-carrier density exceeds the equilibrium majority-carrier density, indicating that the wire arrays were under high-level injection conditions under 1 Sun illumination.

In addition, the arrays exhibited photoanodic behavior in contact with $Me_2Fc^{+/0}$–CH_3OH even though the wires were slightly p-type in doping. This behavior indicates that the *J–E* behavior of the arrays was not dominated by their background doping levels, but instead was dominated by the formation of carrier-selective contacts at the back of the wire through the n^+ substrate as well as through the conformal, high barrier-height contact to the $Me_2Fc^{+/0}$ electrolyte. The combinations of electrochemical experiments and variation of the growth substrate demonstrated that the back contact of the array, in addition to the electrochemical junction, ultimately determined the photoresponse of the wires. These kinetic asymmetries introduced into the wires by the liquid junction and the back contact were critical to achieving a photoresponse in the microwires. This behavior is analogous to previous observations for p–i–n type Si cells in contact with non-aqueous redox systems.[32] As predicted, no photoresponse was observed for arrays with back contacts that were selective for the same carrier type selected by the radial solution contact (*e.g.* n^+ back contacted samples where the electron was collected radially by an electrochemical contact with a relatively negative Nernstian solution potential).

Photoelectrodes formed using n^+/i-Si microwires in contact with $Me_2Fc^{+/0}$–CH_3OH exhibited diode quality factors of $n \sim$ 1.8–2.0, which is characteristic of devices operating under high-level injection conditions. Diode quality factors of ~2.0, ranging from n = 1.6–1.8, have been measured previously for planar p–i–n concentrator devices in contact with $Me_2Fc^{+/0}$–CH_3OH.[12,13] In contrast, previous measurements of p-type Si microwire arrays and of diffused radial junction n^+p-Si microwire arrays have reported diode quality factors closer to 1.0. Arrays of p-Si microwires in contact with the one-electron redox couple methyl viologen, $MV^{2+/+}$, have displayed n = 1.5–1.6 whereas Pt/n^+p-Si wire arrays in contact with aq. 0.5 M H_2SO_4 display n = 1.10 ± 0.04.[5,31] Single-wire radial p–n junctions have exhibited n values between 1.0 and 1.2, consistent with expectations for high-quality, low-recombination p–n junctions operating under low-level injection conditions.[34]

B. Open-circuit photovoltages of n^+/i-Si/$Me_2Fc^{+/0}$ microwire array contacts *vs.* p^+/i-Si $CoCp_2^{+/0}$–CH_3CN microwire array contacts

The p^+/i-Si microwires in contact with $CoCp_2^{+/0}$–CH_3CN typically produced lower V_{oc} values than their n^+/i-Si/$Me_2Fc^{+/0}$ counterparts. This slight difference in the photoresponse was consistent with differences in the effective surface recombination velocities for Si in contact with these redox couples. Specifically $S \sim 20$ cm s^{-1} and $S \sim 55$ cm s^{-1} has been observed for Si in contact with the $Me_2Fc^{+/0}$–CH_3OH and $CoCp_2^{+/0}$–CH_3CN redox systems, respectively.[14] Even for planar n-type and p-type Si photoelectrodes, the n-Si/$Me_2Fc^{+/0}$–CH_3OH contact typically produces higher V_{oc} values than p-Si/$CoCp_2^{+/0}$–CH_3CN contacts.[35–37] p-Si with a resistivity of ~0.24 Ω cm in contact with $CoCp_2^{+/0}$–CH_3CN has produced V_{oc} values of ~540 mV, while n-Si with the same dopant density measured in contact with $Me_2Fc^{+/0}$–CH_3OH has produced V_{oc} values of ~635 mV. In addition, redox couples with more negative electrochemical potentials, such as 1,1′-dimethylcobaltocene$^{+/0}$ in acetonitrile, have elicited higher V_{oc} values from p-Si, demonstrating that the cobaltocene$^{+/0}$ redox system is not completely optimized to produce the maximum photoresponse for photocathodes made using Si/liquid contacts.

C. Carrier-collection efficiency of n^+/i-Si/$Me_2Fc^{+/0}$ microwire devices

The measured internal quantum yield of the wires deviated from unity, consistent with device physics simulations of lightly doped n-Si microwires in contact with $Me_2Fc^{+/0}$–CH_3OH. The measured Γ_{int} showed no change between as-grown wires that had the Cu/Si interfacial region present and polished Si microwires for which this silicide had been removed. Deviations from unity in the observed internal quantum yield can therefore be attributed to the limiting axial transport of electrons in the inverted microwires. The relatively high carrier-collection efficiency of the n^+/i-Si/$Me_2Fc^{+/0}$–CH_3OH system, with experimentally measured peak Γ_{int} values of ~0.8, confirms that the Cu VLS-grown Si microwires were of high electronic quality, with lifetimes exceeding 1 μs.

The device physics simulations provide insight into the photoresponse of the n^+/i- and p^+/i-Si devices, given that the wires should be depleted in contact with the electrolytes used in this work. The simulations of lightly doped n-Si wires in radial

contact with $Me_2Fc^{+/0}$ showed that the wires were depleted of electrons, with a hole-rich inversion layer in the near-surface region, ~100 nm in depth into the wires. As a consequence, the carrier-collection efficiency of the devices was strongly dependent on the radial dimensions of the wire. Small diameter (d < 200 nm) wires should exhibit extremely low quantum yield values, due to their strong inversion throughout the radial dimension. In contrast, larger diameter wires (d > 400 nm) should not be strongly inverted in the core of the wire, providing a collection pathway for electrons that is relatively free of holes, thus resulting in larger, near-unity quantum yields for wires with lifetimes >5 μs. Under the simulation conditions, wires with longer lifetimes demonstrated increasing carrier-collection efficiencies. This trend can potentially be attributed to the higher carrier lifetimes allowing for a smaller recombination rate for electrons transported axially down the wire.

The detailed simulations described herein are in accord with the conclusions reached previously on the conditions required to obtain excellent carrier collection from wire systems that are depleted.[38] Specifically, several conditions must be met for the minority-carrier lifetime in the bulk τ_{bulk} and the surface-based lifetime τ_{surf}. The minority-carrier lifetime in the bulk must satisfy the condition that $\tau_{bulk} > l^2/D_{min}$, where D_{min} is the minority-carrier diffusion coefficient and l is the length of the wire. The surface-based lifetime, $\tau_{surf} = d/2S$ (where d is the diameter of the wire and S is the surface recombination velocity), of the wire must be comparable to, or exceed τ_{bulk}. Hence in addition to $L_{min} > l$, efficient device operation requires that a stringent condition on the surface recombination velocity must be met:

$$S < \frac{Dd}{2l^2} \quad (4)$$

Given the present Si microwire system under investigation, τ_{bulk} must exceed ~1 μs, in agreement with the results for the device physics modeling presented herein, and S < 90 cm s^{-1}, which should be attainable for Si in contact with the solutions employed experimentally in this work. The experimental data and simulations in the present work describing the operation of Si microwires under high-level injection conditions confirm this previous semi-quantitative analysis, and extends it into additional analytical detail.

Despite the potential limitations in carrier transport, the n^+/i-Si microwire arrays in contact with $Me_2Fc^{+/0}$–CH_3OH operating under high-level injection conditions exhibited both *J–E* behavior and external quantum yields similar to those of optimally doped p-Si microwire array photocathodes. A device designed to operate in high-level injection, which could include solid-state radial junction p–i–n Si microwire arrays, has the advantage of increased process simplicity, obviating the need for doping optimization within the absorber material and calibration within a nano- or microstructured device. However, for devices using lightly doped wires, even if the minority-carrier diffusion length exceeds the radius of the wire, the devices will nevertheless be limited by the transport of the majority carrier to the back contact. To further pursue this device architecture, the wires must be fabricated on the microscale using a material with a moderately long carrier lifetime. In addition, highly selective contacts for both carriers and a low effective surface recombination velocity are required to produce an efficient device. Fabricating devices with shorter wires with heights that are well-matched to the majority carrier diffusion length will allow for a high carrier-collection efficiency, but might result in a decrease in overall efficiency due to a decrease in light absorption within the array. These numerical simulations can be further leveraged to optimize the device geometry of lightly doped, structured semiconductors operating under high-level injection conditions.

V. Conclusions

Experimental measurements and device simulations were employed to elucidate the device performance of lightly doped Si wires operating under high-level injection conditions. The *J–E* behavior of the lightly doped Si wire arrays was determined by both the radial contact and the carrier-selective back contact, with wire arrays exhibiting n-type or p-type behavior depending on the choice of redox system and growth substrate. The operation of the lightly doped microwires under high-level injection conditions yielded open-circuit voltages of 445 ± 13 mV for n^+/i-Si wires in contact with $Me_2Fc^{+/0}$–CH_3OH, and open-circuit voltages of 421 ± 14 mV for p^+/i-Si wires in contact with $CoCp^{+/0}$–CH_3CN, exceeding the maximum photovoltage attainable for this system under low-level injection conditions. Consistent with expectations, the microwire arrays exhibited diode quality factors of ~2 when operated under high-level injection conditions in contact with $Me_2Fc^{+/0}$–CH_3OH. These wires exhibited external quantum yields of 0.23 and internal quantum yields of 0.79 in contact with $Me_2Fc^{+/0}$–CH_3OH, deviating from unity carrier-collection efficiency. Complementary device physics simulations of lightly doped, n-Si wires in radial contact with the $Me_2Fc^{+/0}$–CH_3OH redox system showed that the wires were depleted of electrons, with a hole-rich inversion layer in the near-surface region. Wires with small diameters should exhibit low quantum yields for carrier collection, due to the high concentration of holes throughout the radial dimension limiting the axial transport of electrons. Micron-scale diameter wires similar to those experimentally measured (d > 2 μm) should not be strongly inverted in the core of the wire, and therefore should possess an axial carrier-transport collection pathway for electrons that is relatively free of holes. The simulations predicted that near-unity quantum yields can be obtained in microwires with lifetimes exceeding 5 μs, and indicated that the experimentally measured Si microwires possessed carrier lifetimes greater than 1 μs. Thus, both the experimental measurements and simulations have shown that excellent device performance can be achieved with lightly doped, structured semiconductors, by employing radial structures of micron dimensions and semiconductors of high materials quality.

Acknowledgements

We acknowledge the Department of Energy Office of Basic Energy Sciences grant DOE DE-FG02-03ER15483, and BP for

financial support. NCS acknowledges the NSF for an American Competitiveness in Chemistry postdoctoral fellowship (CHE-1042006). Critical support and infrastructure for this work were provided by the Kavli Nanoscience Institute and the Molecular Materials Research Center at Caltech. The angle-resolved optical characterization work was supported by the US Department of Energy 'Light-Material Interactions in Energy Conversion' Energy Frontier Research Center Award (grant DE-SC0001293).

References

1 M. C. Putnam, S. W. Boettcher, M. D. Kelzenberg, D. B. Turner-Evans, J. M. Spurgeon, E. L. Warren, R. M. Briggs, N. S. Lewis and H. A. Atwater, *Energy Environ. Sci.*, 2010, **3**, 1037–1041.
2 C. E. Kendrick, H. P. Yoon, Y. A. Yuwen, G. D. Barber, H. T. Shen, T. E. Mallouk, E. C. Dickey, T. S. Mayer and J. M. Redwing, *Appl. Phys. Lett.*, 2010, **97**, 143108.
3 M. D. Kelzenberg, D. B. Turner-Evans, M. C. Putnam, S. W. Boettcher, R. M. Briggs, J. Y. Baek, N. S. Lewis and H. A. Atwater, *Energy Environ. Sci.*, 2011, **4**, 866–871.
4 B. Tian, T. J. Kempa and C. M. Lieber, *Chem. Soc. Rev.*, 2009, **38**, 16–24.
5 S. W. Boettcher, E. L. Warren, M. C. Putnam, E. A. Santori, D. Turner-Evans, M. D. Kelzenberg, M. G. Walter, J. R. McKone, B. S. Brunschwig, H. A. Atwater and N. S. Lewis, *J. Am. Chem. Soc.*, 2011, **133**, 1216–1219.
6 E. L. Warren, H. A. Atwater and N. S. Lewis, *J. Phys. Chem. C*, 2013, **118**, 747–759.
7 *Handbook of Photovoltaic Science and Engineering*, ed. A. Luque and S. Hegedus, Wiley, Chichester, 2003.
8 R. F. Pierret, *Advanced Semiconductor Fundamentals*, Pearson Education, Upper Saddle River, 2003.
9 R. M. Swanson, S. K. Beckwith, R. A. Crane, W. D. Eades, Y. H. Kwark, R. A. Sinton and S. E. Swirhun, *IEEE Trans. Electron Devices*, 1984, **31**, 661–664.
10 R. A. Sinton, Y. Kwark, S. Swirhun and R. M. Swanson, *IEEE Electron Device Lett.*, 1985, **6**, 405–407.
11 R. A. Sinton, Y. Kwark, J. Y. Gan and R. M. Swanson, *IEEE Electron Device Lett.*, 1986, **7**, 567–569.
12 A. Kumar and N. S. Lewis, *Appl. Phys. Lett.*, 1990, **57**, 2730–2732.
13 M. X. Tan, C. N. Kenyon, O. Kruger and N. S. Lewis, *J. Phys. Chem. B*, 1997, **101**, 2830–2839.
14 F. Gstrein, D. J. Michalak, W. J. Royea and N. S. Lewis, *J. Phys. Chem. B*, 2002, **106**, 2950–2961.
15 M. D. Kelzenberg, *Silicon Microwire Photovoltaics, California Institute of Technology*, Pasadena, 2010.
16 J. M. Foley, M. J. Price, J. I. Feldblyum and S. Maldonado, *Energy Environ. Sci.*, 2012, **5**, 5203–5220.
17 R. R. LaPierre, *J. Appl. Phys.*, 2011, **109**, 034311.
18 W. J. Royea, D. J. Michalak and N. S. Lewis, *Appl. Phys. Lett.*, 2000, **77**, 2566–2568.
19 P. E. Laibinis, C. E. Stanton and N. S. Lewis, *J. Phys. Chem.*, 1994, **98**, 8765–8774.
20 E. A. Santori, J. R. Maiolo III, M. J. Bierman, N. C. Strandwitz, M. D. Kelzenberg, B. S. Brunschwig, H. A. Atwater and N. S. Lewis, *Energy Environ. Sci.*, 2012, **5**, 6867–6871.
21 E. D. Kosten, E. L. Warren and H. A. Atwater, *Opt. Express*, 2011, **19**, 3316–3331.
22 J. R. Maiolo, H. A. Atwater and N. S. Lewis, *J. Phys. Chem. C*, 2008, **112**, 6194–6201.
23 M. D. Kelzenberg, D. B. Turner-Evans, B. M. Kayes, M. A. Filler, M. C. Putnam, N. S. Lewis and H. A. Atwater, *Nano Lett.*, 2008, **8**, 710–714.
24 N. S. Lewis and M. L. Rosenbluth, in *Photocatalysis: Fundamentals and Applications*, ed. N. Serpone and E. Pelizzetti, Wiley Interscience, New York, 1989, pp. 45–121.
25 M. D. Kelzenberg, S. W. Boettcher, J. A. Petykiewicz, D. B. Turner-Evans, M. C. Putnam, E. L. Warren, J. M. Spurgeon, R. M. Briggs, N. S. Lewis and H. A. Atwater, *Nat. Mater.*, 2010, **9**, 239–244.
26 G. Masetti, M. Severi and S. Solmi, *IEEE Trans. Electron Devices*, 1983, **30**, 764–769.
27 N. Tōyama, *Solid-State Electron.*, 1983, **26**, 37–46.
28 T. Heiser, S. McHugo, H. Hieslmair and E. R. Weber, *Appl. Phys. Lett.*, 1997, **70**, 3576–3578.
29 B. M. Kayes, H. A. Atwater and N. S. Lewis, *J. Appl. Phys.*, 2005, **97**, 114302.
30 S. W. Boettcher, J. M. Spurgeon, M. C. Putnam, E. L. Warren, D. B. Turner-Evans, M. D. Kelzenberg, J. R. Maiolo, H. A. Atwater and N. S. Lewis, *Science*, 2010, **327**, 185–187.
31 E. L. Warren, S. W. Boettcher, M. G. Walter, H. A. Atwater and N. S. Lewis, *J. Phys. Chem. C*, 2011, **115**, 594–598.
32 M. X. Tan, C. N. Kenyon, O. Kruger and N. S. Lewis, *J. Phys. Chem. B*, 1997, **101**, 2830–2839.
33 A. L. Fahrenbruch and R. H. Bube, *Fundamentals of Solar Cells: Photovoltaic Solar Energy Conversion*, Academic Press, 1983.
34 M. D. Kelzenberg, D. B. Turner-Evans, M. C. Putnam, S. W. Boettcher, R. M. Briggs, J. Y. Baek, N. S. Lewis and H. A. Atwater, *Energy Environ. Sci.*, 2011, **4**, 866–871.
35 M. L. Rosenbluth and N. S. Lewis, *J. Am. Chem. Soc.*, 1986, **108**, 4689–4695.
36 M. L. Rosenbluth and N. S. Lewis, *J. Phys. Chem.*, 1989, **93**, 3735–3740.
37 R. L. Grimm, M. J. Bierman, L. E. O'Leary, N. C. Strandwitz, B. S. Brunschwig and N. S. Lewis, *J. Phys. Chem. C*, 2012, **116**, 23569–23576.
38 A. Fitch, N. C. Strandwitz, B. S. Brunschwig and N. S. Lewis, *J. Phys. Chem. C*, 2013, **117**, 2008–2015.

